

# The Carboxy Terminus of EmbC from *Mycobacterium smegmatis* Mediates Chain Length Extension of the Arabinan in Lipoarabinomannan\*<sup>§</sup>

Received for publication, December 28, 2005, and in revised form, May 10, 2006 Published, JBC Papers in Press, May 10, 2006, DOI 10.1074/jbc.M513846200

Libin Shi<sup>‡§</sup>, Stefan Berg<sup>‡</sup>, Arwen Lee<sup>¶</sup>, John S. Spencer<sup>‡1</sup>, Jian Zhang<sup>‡</sup>, Varalakshmi Vissa<sup>‡1</sup>, Michael R. McNeil<sup>‡</sup>, Kay-Hooi Khoo<sup>¶||2</sup>, and Delphi Chatterjee<sup>‡3</sup>

From the <sup>‡</sup>Department of Microbiology, Immunology and Pathology, Colorado State University, Fort Collins, Colorado 80523,

<sup>§</sup>Department of Biochemistry and Molecular Biology, Dalian Medical University, Dalian, Liaoning, China, 116027,

<sup>¶</sup>Institute of Biochemical Sciences, National Taiwan University, Taipei 106, Taiwan, and <sup>||</sup>Institute of Biological Chemistry, Academia Sinica, Taipei 115, Taiwan

D-Arabinofurans, attached to either a galactofuran or a lipomannan, are the primary constituents of mycobacterial cell wall, forming the unique arabinogalactan (AG) and lipoarabinomannan (LAM), respectively. Emerging data indicate that the arabinans of AG and LAM are distinguished by virtue of the additional presence of linear termini in LAM, which entails some unknown feature of the EmbC protein for proper synthesis. In common with the two paralogous EmbA and EmbB proteins functionally implicated for the arabinosylation of AG, EmbC is predicted to carry 13 transmembrane spanning helices in an integral N-terminal domain followed by a hydrophilic extracytoplasmic C-terminal domain. To delineate the function of this C-terminal domain, the *embC* knock-out mutant of *Mycobacterium smegmatis* was complemented with plasmids expressing truncated *embC* genes. The expression level of serially truncated EmbC protein thus induced was examined by EmbC-specific peptide antibody, and their functional implications were inferred from ensuing detailed structural analysis of the truncated LAM variants synthesized. Apart from critically showing that the smaller arabinans are mostly devoid of the linear terminal motif,  $\beta$ -D-Araf(1→2)- $\alpha$ -D-Araf(1→5)- $\alpha$ -D-Araf(1→5)- $\alpha$ -D-Araf, our studies clearly implicate the C-terminal domain of EmbC in the chain extension of LAM. For the first time a full range of arabinan chains as large as 18–22 Araf residues and beyond could be released intact by the use of an endogenous endo-D-arabinanase from *M. smegmatis*, profiled, and sequenced directly by tandem mass spectrometry. In conjunction with NMR studies, our results unequivocally show that the LAM-specific linear termini are an extension on a well defined inner branched Ara-(18–22) core. This hitherto unrecognized

feature not only allows a significant revision of the structural model of LAM-arabinan since its first description a decade ago but also furnishes a probable molecular basis of selectivity in biosynthesis, as conferred by the EmbC protein.

The major components of the mycobacterial cell wall are the mycolyl arabinogalactan-peptidoglycan complex and LAM,<sup>4</sup> which have been the subject of intense research over the last 30 years (for review, see Refs. 1–4). Through this phenomenal volume of work, some unique features pertaining to these components have been clarified. The D-arabinan, a common constituent of both LAM and AG, is a unique homopolymer of about 40–70 D-arabinofuranose (Araf) residues, assembled mostly into stretches of  $-\left[\alpha$ -D-Araf(1→5)- $\alpha$ -D-Araf]<sub>n</sub>- with critically spaced  $\alpha$ 3,5-Araf-branched sites. In AG, the nonreducing termini invariably form a well defined  $[\beta$ -D-Araf(1→2)- $\alpha$ -D-Araf]<sub>2</sub>-3,5- $\alpha$ -D-Araf(1→5)- $\alpha$ -D-Araf motif (5), of which the terminal  $\beta$ -Araf and the penultimate  $\alpha$ 2-Araf serve as the anchoring points for the mycolic acids (6). Two such characteristic terminal Ara<sub>6</sub> motifs with additional  $\alpha$ 5-Araf residues at the reducing end are assembled into a unique Ara<sub>22</sub>-mer, the largest structurally defined arabinan unit to date (7). Up to 3 such units are in turn attached in as yet unknown manner to the 5-position of the 6- $\beta$ -D-galactofuranose residues of the D-galactofuran, located in close proximity to the linker region Rha(1→4)GlcNAc (8, 9).

In contrast to such an elaborate architecture of AG with highly structured arabinan, LAM on the other hand boasts a more heterogeneous structural entity based on several aspects such as charge distribution, size, and additional substituents within the molecule (10–12). A tripartite structure of LAM has been established and shown to consist of an arabinan chain on a mannan backbone with a phosphatidylinositol anchor that

\* This work was supported in part by National Institutes of Health Grant AI-37139 (to D. C.) and AI-33706 (to M. R. M.) and Taiwan National Science Council Grant 94-2311-B-001-071 (to K. K.). The costs of publication of this article were defrayed in part by the payment of page charges. This article must therefore be hereby marked "advertisement" in accordance with 18 U.S.C. Section 1734 solely to indicate this fact.

<sup>§</sup> The on-line version of this article (available at <http://www.jbc.org>) contains supplemental Table I.

<sup>1</sup> Supported by NIAID, National Institutes of Health Grants NO1 AI-25469 and AI-47197.

<sup>2</sup> To whom correspondence may be addressed. E-mail: [kkhoo@gate.sinica.edu.tw](mailto:kkhoo@gate.sinica.edu.tw).

<sup>3</sup> To whom correspondence may be addressed. Tel.: 970-491-7495; Fax: 970-491-1815; E-mail: [delphi@lamar.colostate.edu](mailto:delphi@lamar.colostate.edu).

<sup>4</sup> The abbreviations used are: LAM, lipoarabinomannan; Araf, arabinofuranose; MS, mass spectrometry; EmbC<sub>Δc</sub>, recombinant strains with EmbC derivatives with C-terminal deletions; HSQC, heteronuclear single quantum correlation spectroscopy; HSQC-TOCSY, proton-detected single quantum coherence-filtered total correlation spectroscopy; LM, lipomannan; MALDI-TOF, matrix-assisted laser desorption ionization-time of flight; Msm-arabinanase, endogenous endo-D-arabinanase from *M. smegmatis*; *M. smegmatis*ΔembC, *M. smegmatis* embC knock-out mutant; MOPS, 4-morpholinepropanesulfonic acid; mAb, monoclonal antibody; PIM, phosphatidylinositol mannoside.

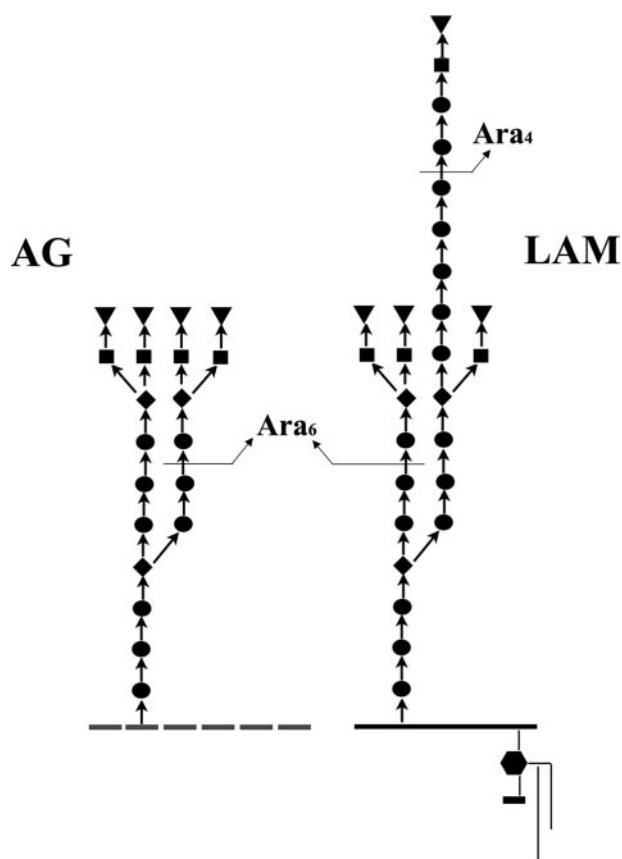


FIGURE 1. **Current structural model of arabinans in LAM and AG.** The symbols represent terminal  $\beta$ -D-Araf ( $\blacktriangledown$ ), 2- $\alpha$ -Araf ( $\blacksquare$ ), 3,5- $\alpha$ -Araf ( $\blacklozenge$ ), and the 5- $\alpha$ -Araf ( $\bullet$ ) residue. The structure and origin of Ara<sub>4</sub> and Ara<sub>6</sub> are shown that would be released with the *Cellulomonas* endoarabinanase. A hallmark of LAM-arabinan is the presence of the linear Ara<sub>4</sub> termini, which are absent in AG. LAM could have a few arabinan chains (not confirmed with data) contributing to its extreme heterogeneity, whereas AG has three well structured arabinan (Ara<sub>22</sub>-mer) attached to the galactan backbone (7).

intercalates into the plasma membrane (Fig. 1). In *Mycobacterium tuberculosis*, the nonreducing ends of these arabinans are capped to varying degrees with mannose residues responsible for much of the LAM biological roles relating to host pathogen interaction. In *M. smegmatis*, a non-pathogen, this capping function is restricted to inositol phosphate on a minor fraction of the termini (13, 14). In addition to the branched nonreducing terminal Ara<sub>6</sub> motif as found in AG, a major difference that identifies the arabinan of LAM from that of AG is the distinctive presence of linear termini (15–17). A commonly held view is to attribute its formation to incomplete  $\alpha$ -3-branching off the  $\alpha$ -5-arabinan backbone before termination by  $\beta$ -2-arabinosylation, thus forming a linear Ara<sub>4</sub>,  $\beta$ -D-Araf(1 $\rightarrow$ 2)- $\alpha$ -D-Araf(1 $\rightarrow$ 5)- $\alpha$ -D-Araf(1 $\rightarrow$ 5)- $\alpha$ -D-Araf, instead of the branched Ara<sub>6</sub> motif. The exact architectural setting and the underlying molecular basis governing their selective biosynthesis are largely unknown except that EmbA and EmbB are involved in this branching.

The genetics and biosynthesis of arabinan remain a gray area even with the availability of the *M. tuberculosis* genome sequence (18). The only biosynthetic information has come from the identification of a two-gene locus from *Mycobacterium avium*, the overexpression of which could render an

otherwise susceptible *M. smegmatis* host resistant to ethambutol (19). Three paralogous genes in an operon encoding putative targets of ethambutol in *M. smegmatis*, *M. tuberculosis*, and *Mycobacterium leprae* were subsequently cloned and sequenced (20, 21). Two of these genes were similar to the *embA* and *embB* described in *M. avium*, as was the third paralog, *embC*, also similar to *embA* and *embB*. Although the Emb proteins have never been isolated nor their functions unequivocally established, critical biochemical analyses have demonstrated that (22) in individual knock-out mutants of *embA* and *embB* in *M. smegmatis*, AG defective at the nonreducing ends (because of the absence of the branched Ara<sub>6</sub> termini) was obtained; whereas the knock-out mutant of *embC* was unable to synthesize any LAM, synthesis of LM remained unaffected (23).

Recent work has identified short amino acid sequences within the Emb proteins that conform to the proline-rich motif found in a family of bacterial membrane proteins known as polysaccharide chain length determinants (24, 25). In addition, Emb proteins have been determined to belong to the glycosyltransferase superfamily C (26). Site-directed mutagenesis of an aspartic acid in the glycosyltransferase superfamily C motif of EmbC led to ablation of LAM synthesis, suggesting an arabinosyltransferase activity (27). Interestingly, introduction of point mutations in the conserved proline motif of EmbC proximal to the C-terminal domain led to synthesis of smaller arabinans largely devoid of linear Ara<sub>4</sub>, thus generating a structure similar to AG. This finding is reminiscent of an earlier work in which replacing the C-terminal domain of EmbC with the corresponding domain of EmbB likewise disfavored the synthesis of linear termini (23).

We hypothesize that the C-terminal domain of the Emb proteins, in contact and perhaps acting in concert with the proximal proline motif, are mainly responsible for selective AG versus LAM-like arabinan formation. Our present work aims to substantiate the contribution of this domain using a recombinant cloning approach to delete various numbers of amino acids from the C-terminal end of EmbC. We demonstrate that C-terminal truncation of EmbC halts LAM-specific linear extension from an AG-like inner arabinan core structure. Collectively, our data reveal a new model that implicates this inner branched Ara-(18–22)-mer core structure as a shared intermediate utilized by enzymes destined for either LAM or AG synthesis.

## EXPERIMENTAL PROCEDURES

**Bacterial Strains and Culture Conditions**—*Escherichia coli* strain DH5 $\alpha$  (Invitrogen) was grown at 37 °C on Luria-Bertani medium with or without ampicillin (100  $\mu$ g/ml), kanamycin (50  $\mu$ g/ml), or hygromycin (50  $\mu$ g/ml). *M. smegmatis* mc<sup>2</sup>155 (22) and recombinant strains were grown at 37 °C in either 7H9 (liquid) or 7H11 (solid, Difco) supplemented with oleic acid-albumin-dextrose-catalase enrichment and glycerol with or without kanamycin (50  $\mu$ g/ml) and hygromycin (50  $\mu$ g/ml). Transformation of *E. coli* was carried out according to standard procedure. Transformation of *M. smegmatis* mc<sup>2</sup>155 was performed by electroporation as described (28).

The status of LAM/LM/PIMs was examined in the total extracts from colonies grown and harvested over 4 days (late

## Arabinan Chain Length Extension in LAM

logarithmic phase to stationary phase for *M. smegmatis*). After 4 days of growth, the cellular content of LAM detected was minimal in all strains. After this observation, to delineate the LAM-arabinan in the mutants, cells were harvested only in log phase (2.5 days for cells cultured in liquid medium).

**Construction of Recombinant Plasmids Encoding the Truncated EmbC Proteins**—The 3225-bp open reading frame of *embC* from *M. smegmatis* was amplified from genomic DNA by PCR using primers (*embC*-f 5'-GTT AGC ATC TAG ACA TAT GAC CGG TCC GCA TGC AG-3'; *embC*-r 5'-AAG CTT CAA CTC AGC CGC AGG GGC GCC GGG-3') including NdeI and HindIII restriction sites (underlined), respectively. The PCR product was cloned into pSTBlue-1 (Novagen) for sequence confirmation and subsequently integrated into pVV16 (derived from pMV261 after digestion with NdeI and HindIII). To construct the recombinant strains with truncated EmbC proteins, the forward primer was combined with one of six reverse primers (listed in supplemental Table 1) for PCR amplification of the desired fragments. The final plasmids were electroporated into *M. smegmatis*Δ*embC* as described (23). The recombinant strains were termed as EmbC<sub>Δ50c</sub>, EmbC<sub>Δ100c</sub>, EmbC<sub>Δ200c</sub>, EmbC<sub>Δ300c</sub>, EmbC<sub>Δ368c</sub>, and EmbC<sub>Δ407c</sub>, symbolizing an increased deletion of amino acids from the C-terminal end of EmbC. On one occasion, the above plasmids were also electroporated into *M. smegmatis* mc<sup>2</sup>155.

**Polyclonal Antibody to *M. smegmatis* EmbC-specific Peptide**—The sequence <sup>162</sup>DDDDPGEAVRGERSGYDFR<sup>180</sup> of *M. smegmatis* EmbC was selected for peptide synthesis based on the following criteria. The peptide shares low or no sequence identity with *M. smegmatis* EmbA, EmbB, and other antigens putatively expressed from the genome of *M. smegmatis* according to BLAST searches performed at The Institute for Genomic Research. Also, the peptide is part of the first predicted loop of *M. smegmatis* EmbC and contains a low number of hydrophobic residues. Peptide (5 mg) was synthesized and conjugated to carrier diphtheria toxoid via the linker maleimidocaproyl-*N*-hydroxysuccinimide (Mimotopes, Roseville, MN). Polyclonal antiserum was raised in BALB/c mice (Harlan, Indianapolis, IN) immunized with an emulsion containing 50 μg of the *M. smegmatis* EmbC peptide coupled to the carrier diphtheria toxoid in a 1:1 ratio of phosphate-buffered saline and incomplete Freund's adjuvant injected at two abdominal sites subcutaneously. Booster injections of 50 μg of antigen in incomplete Freund's adjuvant emulsion were repeated every 3 weeks, with test bleeds taken for enzyme-linked immunosorbent assay after the first and second booster. The titer of the antiserum after the third boost was >1:5000 as measured by Western blot against the native protein enriched in the membrane fraction of *M. smegmatis* or enzyme-linked immunosorbent assay (ELISA) assay by testing serial 2-fold dilutions of the serum against the free peptide (coated on ELISA plate wells at 1 μg/well).

**Detection of EmbC in *M. smegmatis* Wild-type and Recombinant Strains by Western Blot**—Cells were suspended in a buffer containing 50 mM MOPS, 10 mM MgCl<sub>2</sub>, and 5 mM β-mercaptoethanol, pH 8.0, in the presence of protease inhibitor mixture (Sigma) and disrupted by intermittent probe sonication (Soniprep 150, Sanyo Gallenkamp PLC) for 10 cycles (60-s bursts/90

s of cooling). Individual sonicated samples were digested with 10 mg/ml DNase and RNase for 1 h at 4 °C. Cell walls were obtained by centrifugation at 27,000 × *g* for 30 min, and the supernatants from this step were recentrifuged at 100,000 × *g* for 2 h to provide a sediment enriched in membrane. Protein concentration in each of the cell wall, membrane, and cytosolic fractions was determined by BCA assay before subjecting to 10% SDS-PAGE and transferred to nitrocellulose membranes as described (29). The membranes were blocked overnight with 2% bovine serum albumin in Tris-buffered saline incubated with polyclonal mouse serum (1:2000) for 4 h. After washing, the membranes were incubated with anti-mouse IgG-alkaline phosphatase-conjugated antibody (Sigma). The substrates nitro blue tetrazolium and 5-bromo-4-chloro-3-indolylphosphate (Sigma FAST BCIP) were used for color development.

**Extraction of LAM/LM/PIMs from *M. smegmatis* Wild-type and Recombinant Strains**—Cells harvested from 4-liter lots of broth cultures in log phase were washed with phosphate-buffered saline and lyophilized. Dry cells were delipidated with organic solvents and disrupted mechanically with the Soniprep 150. The resulting homogeneous suspension was refluxed in 50% ethanol at 80 °C (3 × 2 h each). The combined supernatants were evaporated and digested with proteinase K (Invitrogen; 1 mg/ml). After dialysis, LAM/LM/PIMs fractions were dried (10, 30).

**Size Fractionation, SDS-PAGE, and Immunoblotting**—For purification of LAM/truncated LAM from all strains used in this study, size exclusion chromatography was performed on a Rainin SD 200 series liquid chromatography system fitted with a Sephacryl S-200 HiPrep 16/60 column in tandem with a Sephacryl S-100 column (Amersham Biosciences) at a flow rate of 1 ml/min (30). SDS-PAGE followed by periodic acid Schiff staining (31, 32) was used to monitor the elution profile of the fractions containing LAM and LM, which were then pooled and dialyzed. Fractions were re-analyzed by SDS-PAGE and immunoblotting with mAb CS-35 as described previously (31) to check for purity before detailed analysis.

**Digestion with Endoarabinanase and Subsequent Analyses**—Preparation of *Cellulomonas gelida* endoarabinanase has been described (5). To ensure complete digestion of LAMs, the reaction mixture was incubated overnight, and the digestion products were analyzed directly by Dionex analytical high pH anion exchange chromatography performed on a Dionex liquid chromatography system fitted with a Dionex Carbopac PA-1 column. The oligoarabinosides were detected with a pulse-amperometric detector (PAD-II) (Dionex, Sunnyvale, CA).

**Monosaccharide Composition**—Samples were hydrolyzed with 2 M trifluoroacetic acid, converted to alditol acetates, and analyzed by gas chromatography (33) on a Hewlett Packard gas chromatography model 5890 fitted with a SP 2380 column (30-m × 0.25-mm inner diameter) at an initial temperature of 50 °C for 1 min, increasing to 170 °C by 30°/min followed by 270 °C by 5 °C/min. Gas chromatography/mass spectrometry (MS) of the methylated alditol acetates were carried out on a ThermoQuest Trace Gas Chromatograph 2000 (ThermoQuest, Austin, TX) connected to a GCQ/Polaris MS mass detector (ThermoQuest). The derivatives were dissolved in hexanes before injection on a DB-5 column

(10-m × 0.18-mm inner diameter, 0.18- $\mu$ m film thickness, J&W Scientific, Folsom, CA) at an initial temperature of 60 °C for 1 min, increasing to 130 °C at 30°/min and finally to 280 °C at 5°/min.

**Digestion with Msm-arabinanase**—Preparation of Msm-arabinanase has been described (34). More recently this enzyme has been sufficiently purified for use as a structural tool via ammonium sulfate precipitation and hydrophobic interaction chromatography (35). Purified LAM (2 mg) from each of the recombinant strains was digested with 250  $\mu$ l of the Msm-arabinanase in 25 mM phosphate buffer at pH 7.0 and incubated for 4 h at 37 °C. The digestion products containing both the mannan core and the released oligoarabinosides were separated using Amicon Microcon YM-30 (Millipore) and centrifuging at 6,500 × *g* for 20 min. The flow-through was then directly permethylated (36) for MS analysis or after further purification by high performance liquid chromatography (Waters) on a Superdex<sup>TM</sup> Peptide 10/300 column (Amersham Biosciences) eluted with water at the rate of 0.5 ml/min. The elution profile was monitored using the Waters refractive index detector, model 2414. The fractions were pooled and analyzed.

**MALDI-MS and MS/MS Analyses**—The arabinan fragments released by Msm-arabinanase were either permethylated or prereduced and permethylated using the NaOH/dimethyl sulfoxide slurry method as described (36). For MALDI-TOF MS glycan profiling, the permethyl derivatives in acetonitrile were mixed 1:1 with 2,5-dihydroxybenzoic acid matrix (10 mg/ml in water) for spotting onto the target plate. MS data acquisition in the reflectron mode was performed on a 4700 Proteomics Analyzer mass spectrometer (Applied Biosystems, Framingham, MA) equipped with an Nd:YAG laser (355-nm wavelength, <500-ps pulse, and 200-Hz repetition rate). MALDI-MS/MS was performed on a dedicated quadrupole TOF Ultima MALDI instrument (Micromass) in which case the permethylated samples in acetonitrile were mixed 1:1 with  $\alpha$ -cyano-4-hydroxycinnamic acid matrix (in acetonitrile, 0.1% trifluoroacetic acid, 99:1 v:v) for spotting onto the target plate. The nitrogen UV laser (337-nm wavelength) was operated at a repetition rate of 10 Hz under full power (300  $\mu$ J/pulse). MS survey data were manually acquired, and the decision to switch over to collision-induced dissociation MS/MS acquisition mode for a particular parent ion was made on-the-fly upon examination of the summed spectra. Argon was used as the collision gas with a collision energy manually adjusted (between 50~200 V) to achieve optimum degree of fragmentation for the parent ions under investigation.

**NMR Spectroscopy of LAM Samples**—Spectra were acquired after several lyophilizations in D<sub>2</sub>O of 4–5 mg/0.6 ml in 100% D<sub>2</sub>O. Two-dimensional <sup>1</sup>H,<sup>13</sup>C{<sup>13</sup>C} heteronuclear single quantum correlation spectroscopy (HSQC) NMR spectra were acquired on a Varian Inova 500 MHz NMR spectrometer (NIH-SIG RR11981) using the supplied Varian pulse sequences. The HSQC data were acquired with a 7-kHz window for proton in F2 and a 15-kHz window for carbon in F1. The total recycle time was 1.65 s between transients. Composite pulse, GARP, decoupling was applied to carbon during proton acquisition. Pulsed field gradients were used throughout for artifact suppression but were not used for coherence selection. The data set

consisted of 1000 complex points in t2 by 256 complex points in t1 using States-TPPI. Forward linear prediction was used for resolution enhancement to expand t1 to 512 complex points. Cos<sup>2</sup> weighting functions were matched to the time domain in both t1 and t2, and zero-filling was applied to both t1 and t2 before the Fourier transform. The final resolution was 3.5 Hz/point in F2 and 15 Hz/pt in F1. Two-dimensional <sup>1</sup>H,<sup>13</sup>C{<sup>13</sup>C} proton-detected single quantum coherence-filtered total correlation spectroscopy (HSQC-TOCSY). NMR experiments were acquired on a Varian Inova-500 NMR spectrometer using the supplied Varian pulse sequence. The HSQC-TOCSY data were acquired with a 5.5-kHz window for proton in F2 and a 15-kHz window for carbon in F1. The TOCSY mixing time was 0.120 ms applied with a 7-kHz field. The total recycle time was 1.65 s between transients. GARP decoupling was applied to carbon during proton acquisition. Pulsed field gradients were used throughout for artifact suppression but were not used for coherence selection. The data set consisted of 1000 complex points in t2 by 256 complex points in t1 using States-TPPI. Forward linear prediction was used for resolution enhancement to expand t1–512 complex points. Cos<sup>2</sup> weighting functions were matched to the time domain in both t1 and t2, and zero-filling was applied to both t1 and t2 before the Fourier transform. The final resolution was 3 Hz/point in F2 and 15 Hz/point in F1.

## RESULTS

**Expression of C-terminal-truncated EmbC Proteins and Synthesis of Truncated LAM Variants**—A prime focus of this work is to assign functions to the predicted C-terminal domain of the EmbC protein. To this end, primers were designed (supplemental Table 1) to generate a series of EmbC proteins truncated from the C-terminal domain as depicted in Fig. 2. Recombinant plasmids were integrated into *M. smegmatis* $\Delta$ embC (23), and the expression level of the respective differentially truncated EmbC protein was examined by Western blot using a polyclonal antibody generated against the peptide antigen from a part of the first predicted loop of *M. smegmatis* EmbC (residue 162–180, Fig. 2). LAM/LM synthesized were in turn extracted, analyzed by SDS-PAGE (Fig. 3A), and immunoblotted with mAb CS-35 (Fig. 3B), which recognizes the arabinan of LAM (37). As expected, the *M. smegmatis* $\Delta$ embC (Fig. 3, A and B, lane 2) failed to synthesize LAM, evident by a lack of positive periodic acid Schiff staining and negative response with CS-35, which was further substantiated by neutral sugar composition (23), but when complemented with the wild-type *embC* gene (strain designated as EmbC<sub>WT</sub> from here onward), LAM of a larger size (lane 3) than that made by the wild-type strain (lane 1) was observed. Accordingly, a sharp protein band corresponding to 115.0 kDa (theoretical molecular mass of *M. smegmatis* EmbC) was evident by Western blot analysis of the membrane extracts from the wild-type *M. smegmatis*. This band was absent in *M. smegmatis* $\Delta$ embC (Fig. 4 lane 2) or in the strain complemented with pVV16 (lane 3), whereas the EmbC<sub>WT</sub> strain (lane 4) showed a significantly increased level of protein expression (based on staining intensity of the protein band per the same amount of total proteins loaded on the SDS/PAGE) relative to that of the wild-type strain (lane 1).

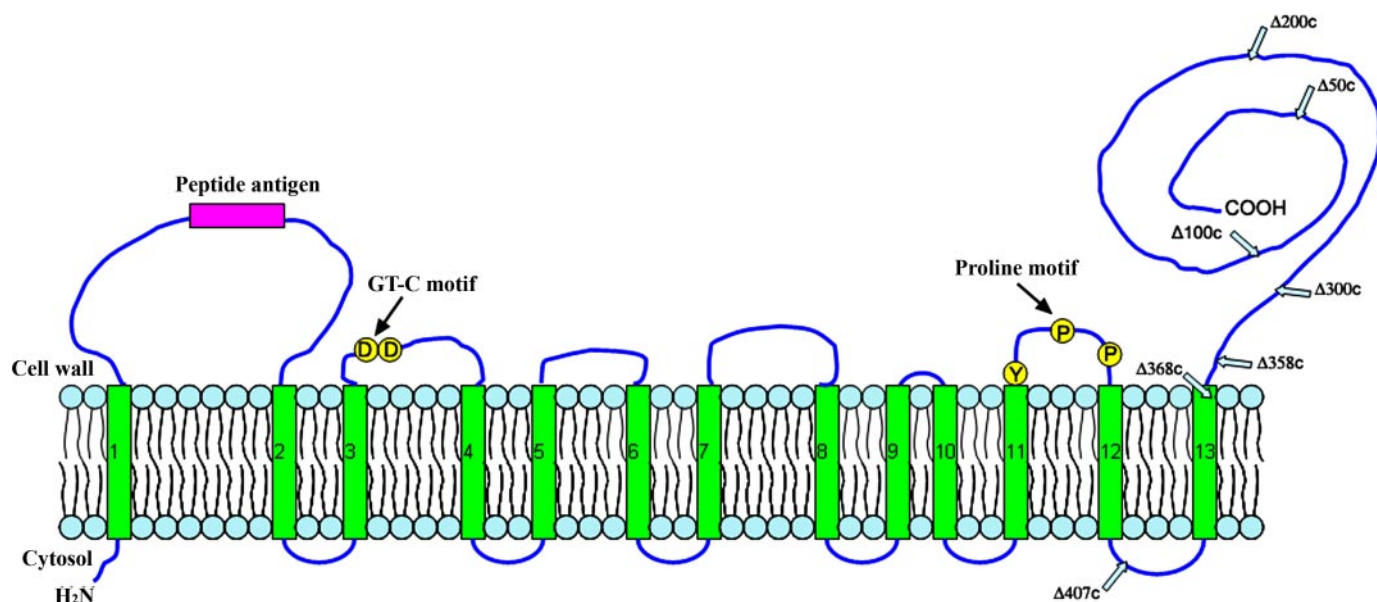


FIGURE 2. Schematic representation of the transmembrane topology of *M. smegmatis* EmbC predicted by Phobius (50), predicted to be a 115.39-kDa protein (1074 amino acids) with 13 transmembrane helices (TMHMM 2.0, Phobius) and a 400-residue C terminus located outside of the membrane. The last four loops have an excess of positively charged residues and are predicted to be on the cytoplasmic side of the membrane (51). The amino acid deletion points from the C-terminal end in the six recombinant EmbC<sub>Δc</sub> constructs are indicated with blue arrows. The Pro motif and the glycosyltransferase superfamily C motif are indicated with circles (27). The peptide sequence highlighted in pink is used to generate antibody and is in the first predicted extracytoplasmic loop.

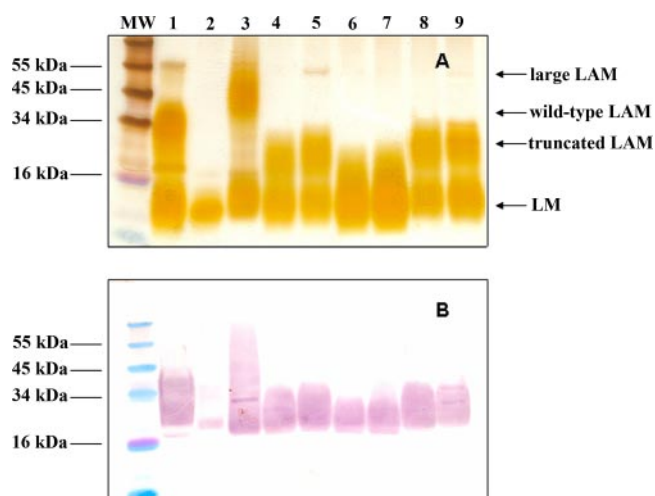


FIGURE 3. Analysis of LAM and LM of wild-type *M. smegmatis* and the mutants by SDS-PAGE (A) and Western blot using mAb CS-35 (B). Molecular mass markers are shown on the left. Lane 1, wild-type *M. smegmatis*; lane 2, *M. smegmatis*ΔembC; lane 3, EmbC<sub>WT</sub>; lane 4, EmbC<sub>Δ50c</sub>; lane 5, EmbC<sub>Δ100c</sub>; lane 6, EmbC<sub>Δ200c</sub>; lane 7, EmbC<sub>Δ300c</sub>; lane 8, EmbC<sub>Δ368c</sub>; lane 9, EmbC<sub>Δ407c</sub>. Two to three colonies were collected from a plate and extracted with 215 μl of solvent (1:1:0.15, chloroform/methanol/water) at 55 °C for 30 min. After centrifugation, the residual pellet was extracted with an equal volume of water (200 μl) and phosphate-buffered saline-saturated phenol (200 μl) at 80 °C for 2 h. The aqueous layer (containing LAM, LM, and PIMs) was dialyzed and analyzed by SDS-PAGE followed by periodic acid Schiff staining and Western blot with CS-35 antibody (23).

An almost equivalent amount of truncated EmbC protein expression was observed for EmbC<sub>Δ50c</sub> and EmbC<sub>Δ100c</sub> (109.5 and 104.0 kDa) at the expected regions of the blot (Fig. 4, lanes 5 and 6). In contrast, protein bands of ~55.0 kDa (lanes 7–10) were obtained for EmbC<sub>Δ200c</sub>, EmbC<sub>Δ300c</sub>, EmbC<sub>Δ368c</sub>, and EmbC<sub>Δ407c</sub>. Thus, truncation beyond the first 200 amino acids from the C terminus apparently compromised its stability, leading to its proteolytic cleavage from the C-terminal end without

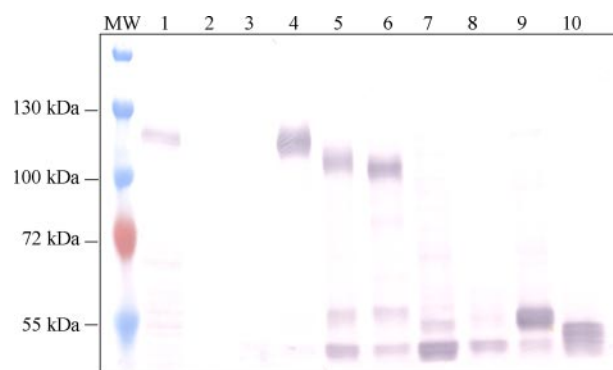


FIGURE 4. Western blot analyses with anti-*M. smegmatis* EmbC peptide antibody. Membrane preparations from strains discussed in this study were used. SDS-PAGE was performed on 10% gel. Lanes 1–3, each with 20 μg of protein; lanes 4–10, each with 3 μg of protein. MW, molecular mass markers; lane 1, wild-type *M. smegmatis*; lane 2, *M. smegmatis*ΔembC; lane 3, *M. smegmatis*ΔembC complemented with pV16; lane 4, *M. smegmatis*ΔembC complemented with the wild-type embC; lane 5, EmbC<sub>Δ50c</sub>; lane 6, EmbC<sub>Δ100c</sub>; lane 7, EmbC<sub>Δ200c</sub>; lane 8, EmbC<sub>Δ300c</sub>; lane 9, EmbC<sub>Δ368c</sub>; lane 10, EmbC<sub>Δ407c</sub>.

significantly affecting its expression level. It is, however, most likely that the respective EmbC proteins were either degraded immediately post-translation or once extracted out from their natural environment after disruption, as all of the deletion derivatives led to some smaller proteolytic products. All the recombinant strains expressing truncated EmbC were found to synthesize truncated LAM (Fig. 3, lanes 4–9), which retained a strong positive response to mAb CS-35 (Fig. 3B). This antibody is known to react more avidly with the branched terminal Ara<sub>6</sub> motif of mycobacterial arabinans present in both AG and LAM that encompasses the minimal recognition epitope, β-D-Araf(1→2)-α-D-Araf(1→5)-α-D-Araf(1→5)-α-D-Araf moiety (37). Thus, C-terminal truncation of EmbC up to about 400 amino acids or so led to impaired synthesis of LAM but did not alter the underlying arabinosyl epitope as defined by mAb

CS-35. To rule out if the smaller proteolytic products (~55.0 kDa) leads to the altered size distribution in LAM, *M. smegmatis* mc<sup>2</sup>155 was transformed with the plasmids harboring EmbC derivatives with C-terminal deletions, and LAM/LM were extracted and analyzed by SDS-PAGE (Fig. 5). LAM of a larger size was formed in the strain with wild-type *embC* gene (Fig. 5, lane 3); however, with all of the EmbC C-terminal-truncated proteins, wild-type LAM phenotype (Fig. 5, lanes 4–9) was obtained. This result suggested that expression of C-terminal-deleted proteins had no negative effect on the EmbC function.

**Isolation and Analysis of LAM**—To further characterize the effects of EmbC C-terminal truncation, LAM/LM were extracted from 4-liter cultures of the recombinant strains and subjected to size exclusion chromatography. Fractions corresponding to LAM/truncated LAMs were pooled after visualization by SDS-PAGE, and the ratio of Ara to Man was determined by neutral sugar composition analysis (Table 1). As a reference standard, LAM isolated from wild-type *M. smegmatis* was shown to contain an Ara to Man ratio of 2.6 or, after normalization based on 1 inositol/mol of LAM, a total of 74 Ara and 28 Man residues. In comparison, LAM isolated from the EmbC<sub>WT</sub> (*M. smegmatis*Δ*embC*-complemented with wild-type *embC*) is composed of 113 Ara and 29 Man residues per inositol, in agreement with its lower electrophoretic mobility relative to the others (Fig. 3). Deletion of the last 50 amino acids from the C-terminal domain of EmbC had a dramatic effect on the Ara content, with a loss of almost 65% of total Ara (40 Ara:25 Man). The total Ara contents decreased further, although not significantly, with the deletion of additional blocks of amino acids from the C-terminal end (100, 200, and 300 residues). This indi-

cated that a deletion of up to 300 amino acids from the C-terminal domain of EmbC did not affect the assembly of mannan but drastically reduced the Ara content and placed a premium on the first 50 amino acids. Further deletion as in EmbC<sub>Δ368c</sub> and EmbC<sub>Δ407c</sub> with almost the entire C-terminal region deleted (Fig. 2) also yielded truncated LAM but with a reduced electrophoretic mobility compared with those of the other mutants (Fig. 3A). Accordingly, their Ara:Man ratio were found to be higher and, per mol of inositol, gave an Ara content more resembling that of wild-type LAM (Table 1). Thus, the innermost segment of the C-terminal domain may impose additional biosynthetic regulation or selectivity constrain distinct from that exerted by the last 50 amino acids. However, it is also conceivable that amino acid deletions in the C-terminal end have effects on folding of the remaining protein containing a single important domain.

**Nonreducing Terminal Arabinan Motifs**—Enzymatic digestion with an endoarabinanase preparation from *Cellulomonas* has been shown to consistently release the nonreducing end Ara<sub>6</sub> and Ara<sub>4</sub> from the arabinan in LAM (5, 16) along with the digestion of the inner core into a dimeric Ara<sub>f</sub>-(1→5)-α-Ara<sub>f</sub> (Ara<sub>2</sub>). Thus, a hallmark of digestion with this enzyme is the yield of linear terminal Ara<sub>4</sub> and branched terminal Ara<sub>6</sub> from LAM but only Ara<sub>6</sub> from AG. To investigate if the nonreducing termini of the truncated LAM produced by the recombinant strains were altered, their endoarabinanase digestion products were profiled by Dionex high pH anion exchange chromatography (Fig. 6) and MS analysis. Notably for all recombinant strains investigated, the levels of Ara<sub>4</sub> (representative of the linear nonreducing termini of LAM) relative to that of Ara<sub>6</sub> decreased by almost 60–70%.

MALDI-MS profiling of the per-*O*-acetyl derivatives of the enzyme digestion products from wild-type LAM afforded a series of sodiated molecular ions corresponding to Ara<sub>2–9</sub>, with the two most prominent ones at *m/z* 989 and 1421 corresponding to Ara<sub>4</sub> and Ara<sub>6</sub>, respectively. In LAMs from EmbC<sub>Δc</sub> strains the relative intensity of the Ara<sub>4</sub> ion diminished noticeably to residual level, whereas the Ara<sub>6</sub> ion was consistently present as the major molecular ion, thus corroborating the high pH anion exchange chromatography profile (data not included).

**Distinctive Structural Features of Wild-type LAM and EmbC<sub>Δ200c</sub> LAM by NMR Analyses**—For structural investigation using NMR, we selected LAM isolated from the EmbC<sub>Δ200c</sub> solely based on the compositional analyses (Ara:Man ratio, Ara<sub>4</sub>/Ara<sub>6</sub> ratio, electrophoretic mobility). Methylation analy-

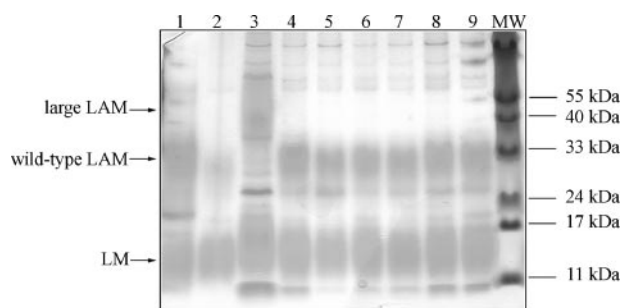


FIGURE 5. Analysis of LAM and LM from *M. smegmatis* mc<sup>2</sup>155 transformed with plasmids as described in Fig. 3 by SDS-PAGE and periodic acid Schiff staining. MW, molecular weight markers. Lane 1, wild-type *M. smegmatis*; lane 2, *M. smegmatis*/pVV16; lane 3, *M. smegmatis* transformed with wild-type *embC*; lanes 4–9, *M. smegmatis* transformed with vectors expressing C-terminal deletions as in Δ50c, Δ100c, Δ200c, Δ300c, Δ368c, and Δ407c.

TABLE 1

Compositional analysis of *M. smegmatis* wild-type LAM and truncated LAMs from the EmbC<sub>Δc</sub> constructs

The analysis was repeated five times for each set before confirming the molar ratios presented in this experiment (variation in molar ratios were within ±10%). The data presented are from one set of experiments.

Strains	Ara	Ara % change	Man	Man % change	Myo-Ins	Ara/Man ratio
Wild-type LAM	74	NA	28	NA	1	2.63
EmbC <sub>WT</sub> <sup>a</sup>	113	100	29	100	1	3.89
EmbC <sub>Δ50c</sub>	40	-64.6	25	-10.7	1	1.60
EmbC <sub>Δ100c</sub>	40	-64.6	26	-7.1	1	1.53
EmbC <sub>Δ200c</sub>	31	-72.5	22	-21.4	1	1.41
EmbC <sub>Δ300c</sub>	35	-69.0	25	-10.7	1	1.40
EmbC <sub>Δ368c</sub>	75	-33.6	35	+25.0	1	2.14
EmbC <sub>Δ407c</sub>	71	-37.1	37	+32.1	1	1.92

<sup>a</sup> To reflect the percentage change in Ara and Man content in LAM preparations, the Ara and Man in EmbC<sub>WT</sub> was considered as 100%.

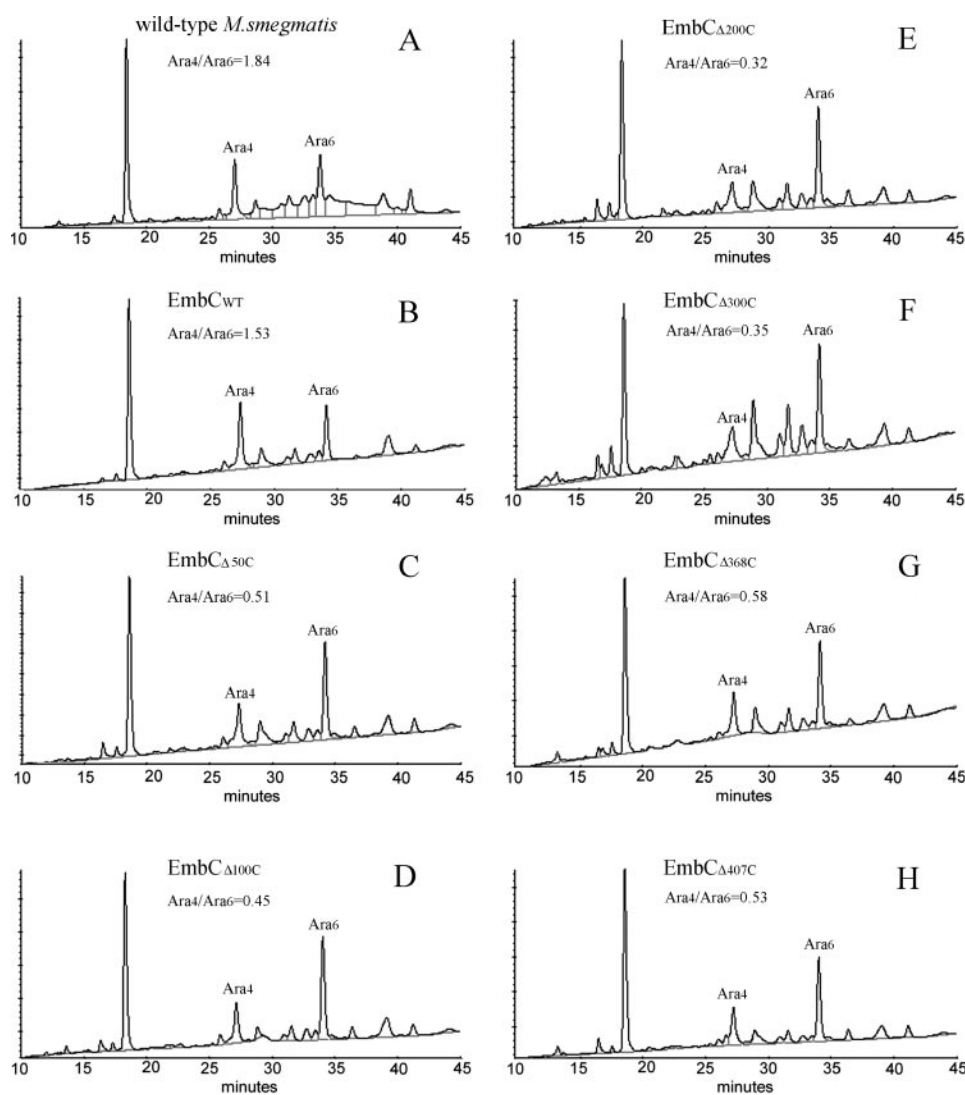


FIGURE 6. Dionex high pH anion exchange chromatography profiles of endoarabinanase-digested fragments. Oligomers were produced from LAM from wild-type *M. smegmatis* and mutants. Samples (10  $\mu$ g each) were digested with the *Cellulomonas* enzyme (5). The major peaks were all confirmed after per-*O*-acetylation and MALDI/TOF mass spectral analyses. The ratio of  $Ara_4/Ara_6$  was determined from the relative intensity (area) of the peaks.

sis revealed that the arabinan comprises t-Araf, 3,5-Araf, 5-Araf, and 2-Araf units (data not shown). By comparing the  $^{13}\text{C}, ^1\text{H}$  heteronuclear NMR spectra from wild-type LAM (Fig. 7A) and EmbC $_{\Delta 200\text{C}}$  LAM (Fig. 7B) and in agreement with previous studies that report two-dimensional NMR of wild-type LAM (38, 39), the overall arabinan domain seemed to hold in the mutant. The NMR parameters are consistent with the methylation analyses albeit with notable differences (Fig. 7B). There were altogether seven well differentiated and one overlapping spin system distributed in the anomeric region ( $\delta 100$ – $\delta 109.3$  ppm). Based on the literature (12, 38–41), the  $^{13}\text{C}$  resonance at  $\delta 100.89$  ppm that correlated to anomeric protons at  $\delta 5.13$  ppm with  $^1J_{\text{H}_1, \text{C}_1}$  coupling constants of  $\sim 170$  Hz was attributed to the 2,6- $\alpha$ -mannopyranose. t- $\alpha$ -mannopyranose resonated at  $\delta 104.9$  ppm and correlated to protons at  $\delta 5.06$  ppm. The cross-peak at  $\delta 102.15$  ppm correlating with  $^1\text{H}$  at  $\delta 4.92$  was assigned to 6- $\alpha$ -mannopyranose and was weak due to saturation of the water peak around the same region. Two completely overlapping sets of cross-peaks centered at  $\delta 103.35$

with  $^1\text{H}$  at  $\delta 5.16$  corresponded to the t- $\beta$ -Araf. Two well separated spin systems were identified for 2- $\alpha$ -Araf (cross-peaks for overlapping C-2 were detected at  $\delta 88.7$ ), namely those attached to the 3-position (2- $\alpha$ -Araf $\rightarrow$ 3,  $\delta 108.19$ ,  $\delta 5.27$  ppm) and 5-position (2- $\alpha$ -Araf $\rightarrow$ 5,  $\delta 108.44$ ,  $\delta 5.19$  ppm) of the 3,5- $\alpha$ -Araf.

As expected, multiple distinct spin systems were observed centered between  $\delta 110.4$  and  $\delta 109.5$  ppm, correlating with protons between  $\delta 5.11$  and  $\delta 5.18$  ppm. These were all attributed to the 5- $\alpha$ -Araf in different chemical environments overlapping with one set of 3,5- $\alpha$ -Araf ( $\delta 5.18$ – $5.11$ ). Most of the resonances in the HSQC spectrum obtained from EmbC $_{\Delta 200\text{C}}$  LAM (Fig. 7B) were in agreement with those assigned for wild-type LAM (Table 2) except for two additional cross-peaks centered at  $\delta 109.7$ ,  $^1\text{H}$  at  $\delta 5.25$  ppm and  $^{13}\text{C}$  at  $\delta 110.63$  with  $^1\text{H}$  at  $\delta 5.04$  ppm. The chemical shift ranging between  $\delta 110$  and  $\delta 108$  was supportive of the  $\alpha$ -anomeric configuration of the Araf residues. The cross-peaks at  $\delta 5.25$  and  $\delta 5.04$  ppm were new ( $\delta\text{C}$  109.7 and 110.63), which could be attributed to terminal  $\alpha$ -Araf (42) arising from incomplete  $\beta$ 2-arabinosyl termination of a growing arabinan chain. Two distinct chemical shifts of t- $\alpha$ -Araf could occur for the respective two arms of a branched

3,5- $\alpha$ -Araf, as observed for the resonances of 2- $\alpha$ -Araf $\rightarrow$ 5 and 2- $\alpha$ -Araf $\rightarrow$ 3. Indeed, the chemical shifts recorded for the two putative t- $\alpha$ -Araf matched completely to those afforded by a synthetic pentasaccharide acceptor, octyl  $\alpha$ -Araf(1 $\rightarrow$ ) $_2$ -3,5- $\alpha$ -Araf-(1 $\rightarrow$ 5)- $\alpha$ -Araf-(1 $\rightarrow$ 5)- $\alpha$ -Araf.<sup>5</sup> Furthermore, the spin system of the  $\alpha$ -Araf could be defined up to H-5/C-5 from a comparative two-dimensional HSQC-TOCSY experiment on LAM versus the synthetic acceptor. Thus,  $^{13}\text{C}$  chemical shifts of the cross-peaks for H-1/C-2s were detected at  $\delta 84.2$  ppm, and the rest of the chemical shifts collectively proved that this unit was terminal. The furanose ring was deduced from the C-4 chemical shift ( $\delta 86.7$ ) and the cross-peak observed between H-1 ( $\delta 5.25$ ) and C-4 ( $\delta 86.7$ ). For 2- $\alpha$ -Araf $\rightarrow$ 3 and 2- $\alpha$ -Araf $\rightarrow$ 5 the  $^{13}\text{C}$  chemical shift was found to be at  $\delta 88.7$  ppm.

These rarely observed structural features are in accord with a working model of attributing LAM truncation to incomplete or

<sup>5</sup> J. Zhang and D. Chatterjee, unpublished work.

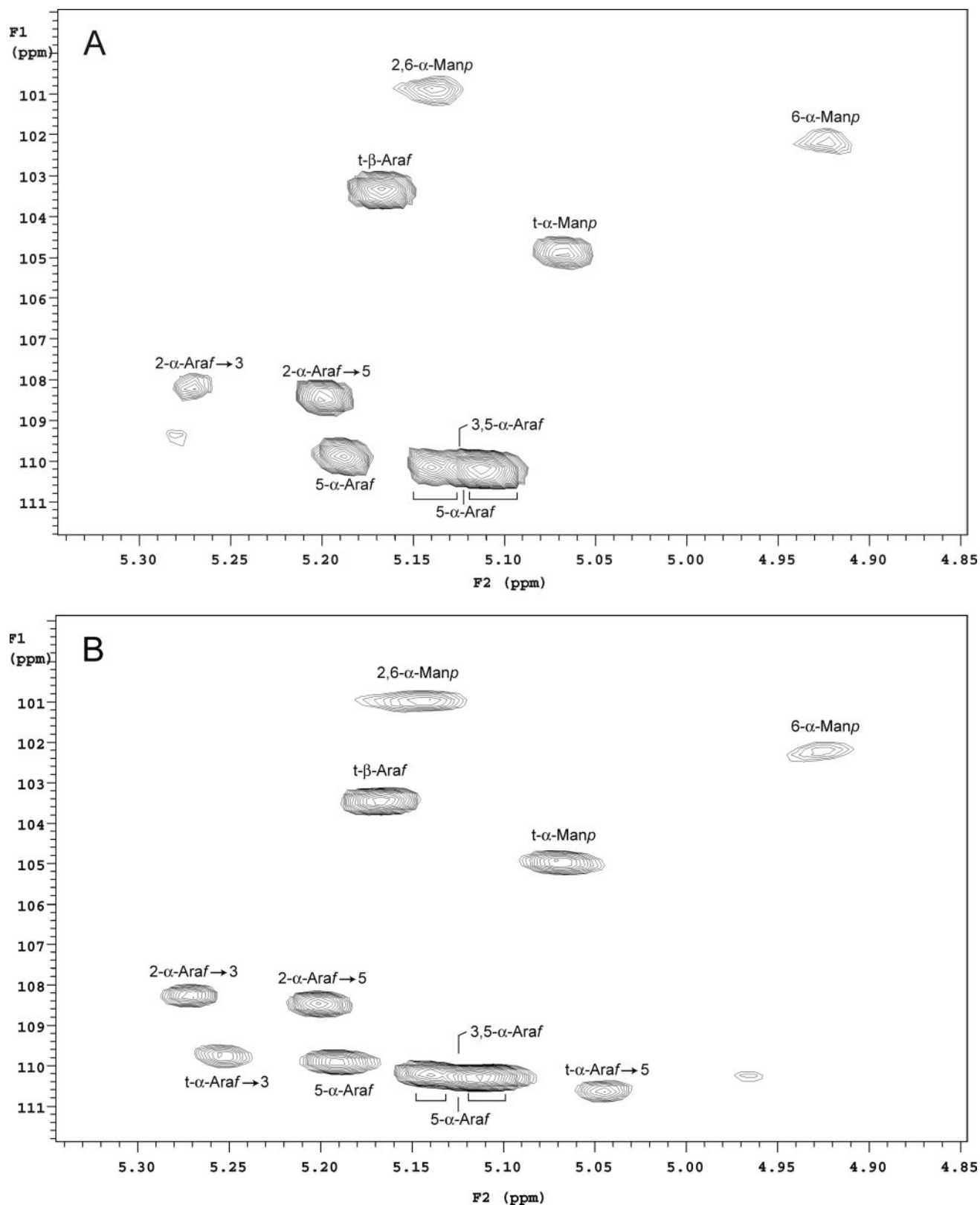


FIGURE 7. **Comparative partial two-dimensional NMR spectra of LAM purified from wild-type *M. smegmatis* (A) and *EmbC* $_{\Delta 200c}$  (B).**  $^1\text{H}$ ,  $^{13}\text{C}$  HSQC spectra were acquired in  $\text{D}_2\text{O}$ . Only the expanded anomeric regions are shown ( $^1\text{H}$ ,  $\delta 4.60$ – $\delta 5.05$  ppm, and  $^{13}\text{C}$ ,  $\delta 98$ – $\delta 110.5$  ppm). t- $\alpha$ -Araf was assigned from chemical shift and a separate HSQC-TOCSY experiment (data not shown).

reduced linear extension of an underlying branched arabinan framework, manifested as apparent lack or diminished expression of linear Ara<sub>4</sub> terminal motif relative to the branched Ara<sub>6</sub>

motif. A comparative NMR analysis of LAM produced by a hybrid Emb protein carrying the two-thirds of the N terminus of EmbC and one-third of the C terminus of EmbB afforded a

## Arabinan Chain Length Extension in LAM

**TABLE 2**  
<sup>1</sup>H-, <sup>13</sup>C NMR chemical shift assignment based on two-dimensional HSQC of LAMs from wild-type *M. smegmatis* and EmbC<sub>Δ200c</sub>  
 Chemical shifts were measured in D<sub>2</sub>O at 500 MHz, 295 K. ND, not determined.

Glycosyl residues	<i>M. smegmatis</i> LAM		EmbC <sub>Δ200c</sub> LAM	
	<sup>13</sup> C	<sup>1</sup> H	<sup>13</sup> C	<sup>1</sup> H
t-β-Araf	103.35	5.16	103.44	5.16
2-α-Araf→3	108.19	5.27	108.26	5.27
2-α-Araf→5	108.44	5.19	108.46	5.20
3,5-α-Araf	110.22	5.11	110.28	5.11
t-α-Araf→3	ND	ND	109.70	5.25
t-α-Araf→5	ND	ND	110.63	5.04
5-α-Araf	110.15	5.14	110.2	5.14
5-α-Araf	109.88	5.18	109.90	5.19
t-α-Manp	104.9	5.06	104.95	5.07
6-α-Manp	102.15	4.92	102.19	4.92
2,6-α-Manp	100.89	5.13	100.96	5.14

spectrum identical to the one from EmbC<sub>Δ200c</sub> (Table 2). It has been demonstrated that LAM synthesized by this hybrid likewise had AG-like arabinan with the characteristic linear Ara<sub>4</sub> motif largely missing (23).

**MALDI-MS and MS/MS Mapping of Large Arabinan Fragments Released from LAM by Msm-arabinanase**—Incomplete elaboration of the arabinan due to the deleted functional domain of EmbC would lead to overall truncation in size and, by implication, an altered branching pattern of the subterminal structural domains due to reduced linear extension. We next sought to demonstrate this effect by mapping the large arabinosyl oligomers that would be released from LAM by an endogenous Msm-arabinanase previously shown to release large oligoarabinosyl units from AG (34). The digestion products were filtered through Amicon Microcon YM-30 to remove any large resistant core and proteins. The filtrates were then desalted and permethylated for direct MALDI-MS profiling and MS/MS sequencing.

Although the wild-type LAM afforded a full range of arabinosyl oligomers from Ara<sub>5</sub> to more than Ara<sub>30</sub> (Fig. 8A), the profiles afforded by the EmbC<sub>Δ200c</sub> and EmbC<sub>Δ368c</sub> (Fig. 8, B and C) were distinctively different in several aspects. First, the released arabinosyl oligomers apparently extended only up to Ara<sub>22</sub> or Ara<sub>23</sub>, which would be consistent with an overall smaller arabinan size. Second and more important, instead of a similar abundance for each of the oligomers as in the wild type, the mutants yielded mostly Ara<sub>17–20</sub> as the major products, peaking at Ara<sub>18</sub>. The most pronounced effect was afforded by LAMs isolated from EmbC<sub>Δ200c</sub> and EmbC<sub>Δ358c</sub>, which correspond also to the most severely truncated LAMs as visualized by SDS-PAGE (EmbC<sub>Δ358c</sub> was not included in the SDS-PAGE because its electrophoretic mobility was similar to the EmbC<sub>Δ300c</sub>). Interestingly, this drastic change in arabinosylation pattern was somewhat reversed with further truncation of the C-terminal domain. The corresponding MS profile for EmbC<sub>Δ368c</sub> (Fig. 8Ds) exhibited a pattern more similar to that afforded by the wild-type LAM, albeit still with slightly more abundant Ara<sub>17–20</sub>. The data are, thus, consistent with the findings that its Ara content has increased back to the level approaching that of wild-type LAM (Table 1).

It is tempting to speculate that such an apparent change in the arabinosylation pattern was indeed due to impaired EmbC function in extending the arabinan in a linear manner. Thus,

the Ara<sub>17–20</sub> oligomers would correspond to a fundamental core structure commonly found in both AG and LAM, as defined by previous analysis to be an assembly of two uniquely branched Ara<sub>6</sub> units (43). Supporting data were derived from MS/MS sequencing of each of the arabinosyl oligomers released from the wild-type LAM (Fig. 9) in comparison against a representative set from EmbC<sub>Δ358c</sub> LAM (Fig. 10). To facilitate signal assignment, the samples were first reduced to convert the oligomers to oligoarabinosyl alditols and then permethylated. Each single cleavage induced by MS/MS would generate fragment ions with a free hydroxyl group. A fragment ion, which can only be derived by two cleavages, will be distinguished from the former by virtue of having an additional OH group.

In practice, a linear stretch of arabinosyl chain at the nonreducing end of an oligoarabinosyl alditol is identified by the ability to detect consecutive losses of Ara residues from nonreducing end with single cleavage events. This was indeed the case with each of the oligoarabinosyl alditols derived from wild-type LAM. For example, the loss of a fully methylated nonreducing terminal Ara residue from Ara<sub>8</sub> (*m/z* 1365) yielded the sodiated  $\gamma$  ion at *m/z* 1191. Subsequent losses of Ara residues did not generate additional free OH groups. Thus, loss of 1–6 Ara residues could each occur by single cleavage to afford primary fragment ions at *m/z* 1191, 1031, 871, 711, 551, and 391, respectively. Nevertheless, loss of a third Ara residue (and onward) could also favorably be derived from double cleavages, giving rise to the fragment ion at *m/z* 857 or 14 units (a methyl group) lower than that produced by single cleavage. The data are, therefore, indicative of a significant degree of branching occurring at the third Ara residue from the nonreducing end, which exists along a linear structure (Fig. 9A). The same pattern was observed for all other oligoarabinosyl alditols (Fig. 9, B–D), where losses of as many Ara residues could all occur via single cleavage event, but the existence of branched points was also apparent.

In contrast, a distinctive fragmentation pattern could be observed for the corresponding oligoarabinosyl alditols derived from the LAM of EmbC<sub>Δ358c</sub> (Fig. 10). For Ara<sub>14</sub>, a branched point apparently exists at the ninth Ara residue from the nonreducing end since losses of up to eight but not nine Ara residues from the nonreducing terminus could occur via single cleavage. Instead of prominent pairs of sodiated  $\gamma$  ions at *m/z* 857/871 and 697/711, as afforded by the wild-type LAM (Fig. 9C), the truncated LAM gave mainly *m/z* 857 and 697 (Fig. 10A), indicating a stricter adherence to branching at the expense of linear extension. Alternatively, the branching pattern was made more apparent in the absence of linear extension. Even more strikingly for the Ara<sub>18</sub> (Fig. 10C), single-cleavage loss of three and four Ara residues from the nonreducing terminus was much more disfavored than that afforded by the corresponding Ara<sub>18</sub> from wild-type LAM (Fig. 9D). A drop in intensity was associated with higher abundance of the double cleavage fragment ions at *m/z* 2459 and 2299 relative to those from single cleavage at *m/z* 2473 and 2313. As in Ara<sub>14</sub>, a branched point is again apparent at residue nine from the nonreducing terminus that led to detection of  $\gamma$  ion at *m/z* 1497 instead of *m/z* 1511. The dominant expression of a character-

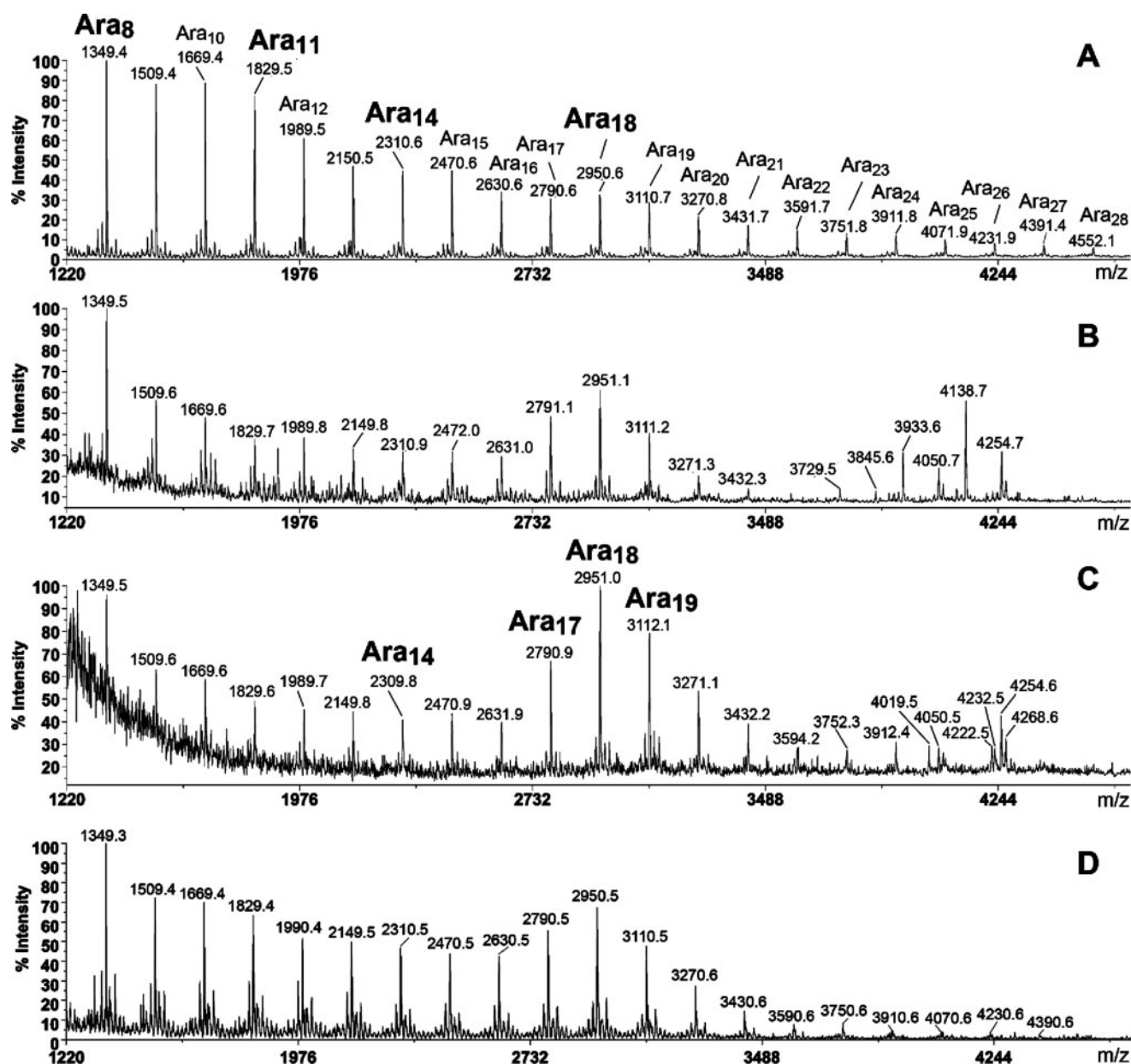


FIGURE 8. MALDI-MS profiling of arabinosyl oligomers released by *Msm*-arabinanase. From wild-type LAM (A) or truncated LAMs from mutants *EmbC* $_{\Delta 200c}$  (B), *EmbC* $_{\Delta 358c}$  (C), and *EmbC* $_{\Delta 368c}$  (D). The corresponding MS profiles of *EmbC* $_{\Delta 100c}$  and *EmbC* $_{\Delta 300c}$  are very similar to that of *EmbC* $_{\Delta 200c}$ , which is shown here as a representative spectrum. For all mutants, *Ara* $_{17-19}$  became the most prominent *Msm*-arabinanase digestion products, and of those investigated, the most pronounced change was afforded by *EmbC* $_{\Delta 358c}$  (C). As shown in B and C, severe truncation led to detection of another cluster of signals at around *m/z* 4000 corresponding to *Ara*- and *Hex*-containing components as could be inferred from their mass intervals. These are likely to be derived from mannan core with remaining *Ara* attached, but their exact identity was not further investigated in this study. With *EmbC* $_{\Delta 368c}$  (D), the profile apparently reverted back to resemble more that afforded by wild-type LAM (A), although *Ara* $_{17-19}$  still registered as the major products. All major arabinosyl oligomers from the digests of wild-type LAM and LAM from *EmbC* $_{\Delta 358c}$  were selected for MALDI-MS/MS analyses, but only the MS/MS spectra for those peaks labeled as *Ara* $_n$  in bold in A and C are shown in Fig. 7 and 8, respectively. *Manp*, mannopyranose.

istic branched terminal *Ara* $_8$  structural motif was likewise observed for the *Ara* $_{17}$  and *Ara* $_{19}$  oligomers. In both cases (Fig. 10, B and D), loss of up to eight but not nine *Ara* residues from the nonreducing termini could occur via single cleavage. Thereafter, single cleavage loss of further *Ara* residues was mostly disallowed except for *Ara* $_{19}$  in which a loss of an *Ara* $_{17}$  moiety could again occur by single cleavage, giving rise to the *y* ion at *m/z* 391. Thus, two *Ara* $_8$  moieties may be co-joined at another branched residue proximal to the reducing end to yield the implicated *Ara* $_{17}$  moiety, as schematically shown in Fig. 10.

Taken together, both MS profile and MS/MS data are consistent with a structural model for the arabinan of LAM in which additional linear  $\alpha$ -5-*Ara* extensions occur on a common *Ara* $_{22}$  oligomeric base, a function largely mediated by the last 350 amino acids of the *EmbC*. In wild-type LAM, such a structural motif would also be present, but the fragmentation pattern of the corresponding *Ara* $_{18}$  was not as distinct since other isomeric structures with linear stretches of oligoarabinosyl chains coexist. A reduced linear extension due to truncation in the C-terminal functional domain of *EmbC* also reduced the

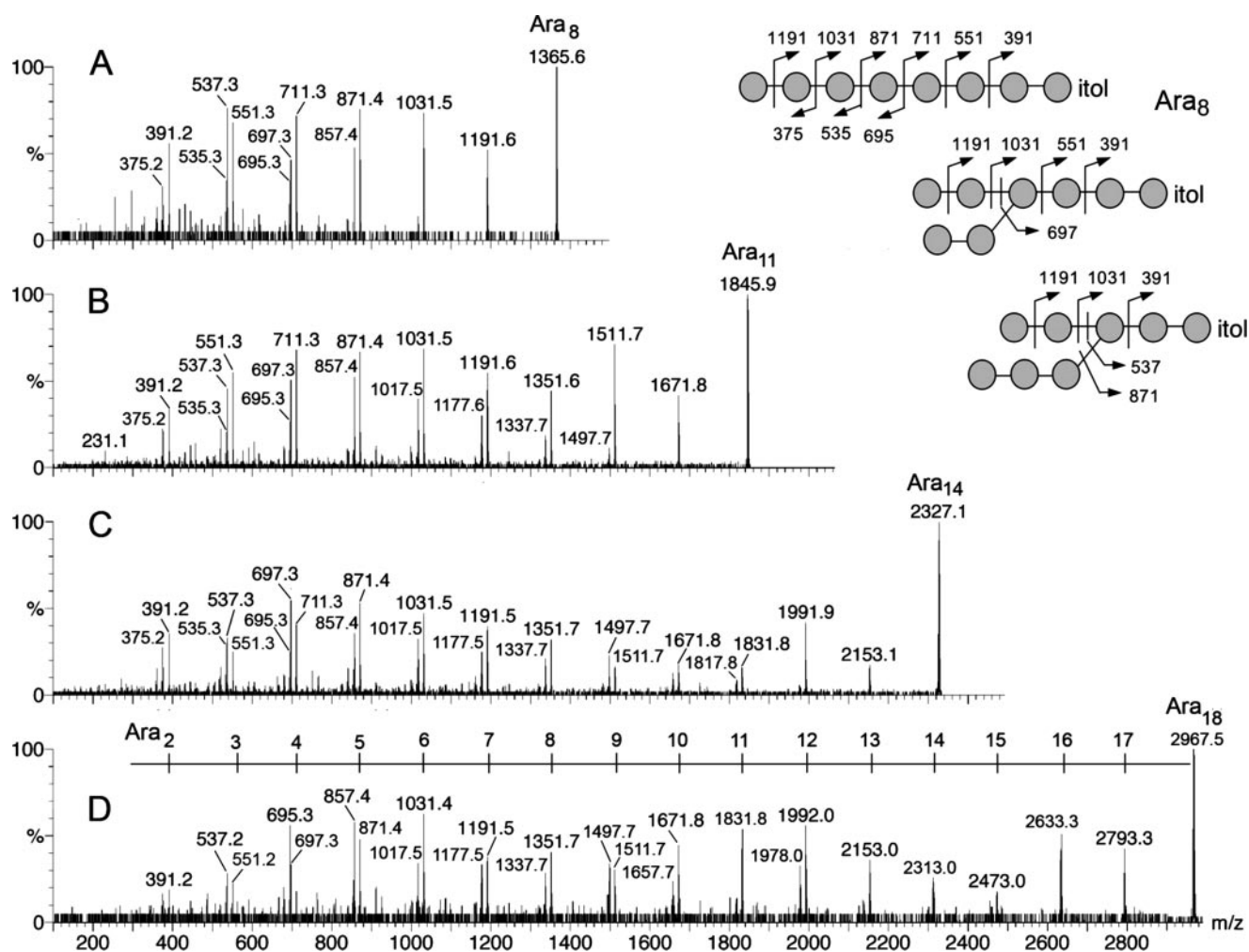


FIGURE 9. MALDI-MS/MS analysis of arabinosyl oligomers derived from *Msm*-arabinanase digested wild-type LAM. Only representative MS/MS spectra on Ara<sub>8</sub>, Ara<sub>11</sub>, Ara<sub>14</sub>, and Ara<sub>18</sub> are shown. The major fragment ions afforded by the sodiated parent ions correspond to sodiated y ions. Additional sodiated c ions were observed at *m/z* 375, 535, and 695, corresponding to Ara<sub>2-4</sub>(OH)<sub>1</sub>. The number of Ara residues represented by each cluster of fragment ions is as indicated by the horizontal scale in D. Both linear and branched structural models of Ara<sub>8</sub> that are consistent with the fragment ions afforded (A) are schematically illustrated. For all arabinosyl oligomers no single unique sequence can be drawn, as the data implicated coexistence of isomeric structures.

overall heterogeneity, leading essentially to a more AG-like arabinan.

### DISCUSSION

The arabinan in mycobacteria has important structural and pathogenic implications. The covalent modification of the arabinan termini of AG with mycolic acids results in an effective lipid barrier, whereas mannose capping of *M. tuberculosis* LAM generates crucial immunomodulatory properties in the host. It is, therefore, a valid therapeutic target because blocking its biosynthesis would disrupt both the cell wall *per se* and its associated biologically active LAM (44–46). However, many of the structural features of arabinan remain incompletely understood, largely due to unavailability of defined mutants and appropriate analytical tools to address its structural complexities.

Until very recently little was known about the genes involved in the arabinan synthesis. Through genetic and biochemical studies, the EmbC protein specifically has now emerged as the candidate LAM-arabinan transferase (23, 27), which in contrast

to the related EmbA and EmbB proteins (destined for AG-arabinan biosynthesis) (21, 22), is reckoned to carry an additional recognition motif that would accommodate the extra degree of flexibility necessary for the synthesis of the extended LAM-type arabinan. To explain the findings that interruption of the *embC* gene leads to a “complete cessation” in the synthesis of the arabinan in LAM but not AG, whereas LM synthesis remains unaffected, we propose that in the LAM arabinan biosynthetic pathway segments of the EmbC are involved in the transfer of crucial preformed polyprenyl-linked arabinan chains. Further delineation of the structure-function aspects of the Emb proteins has, thus, become vital in understanding the enzymology of biosynthesis of LAM and AG.

In our present study we have exploited the “LAMless” phenotype of the knock-out strain *M. smegmatis*Δ*embC* to artificially generate LAM variants by a recombinant cloning approach. Thus, when the LAMless phenotype of the knock-out mutant was rescued with plasmids expressing EmbC derivatives with C-terminal deletions, truncated and structurally altered LAM yet recognized

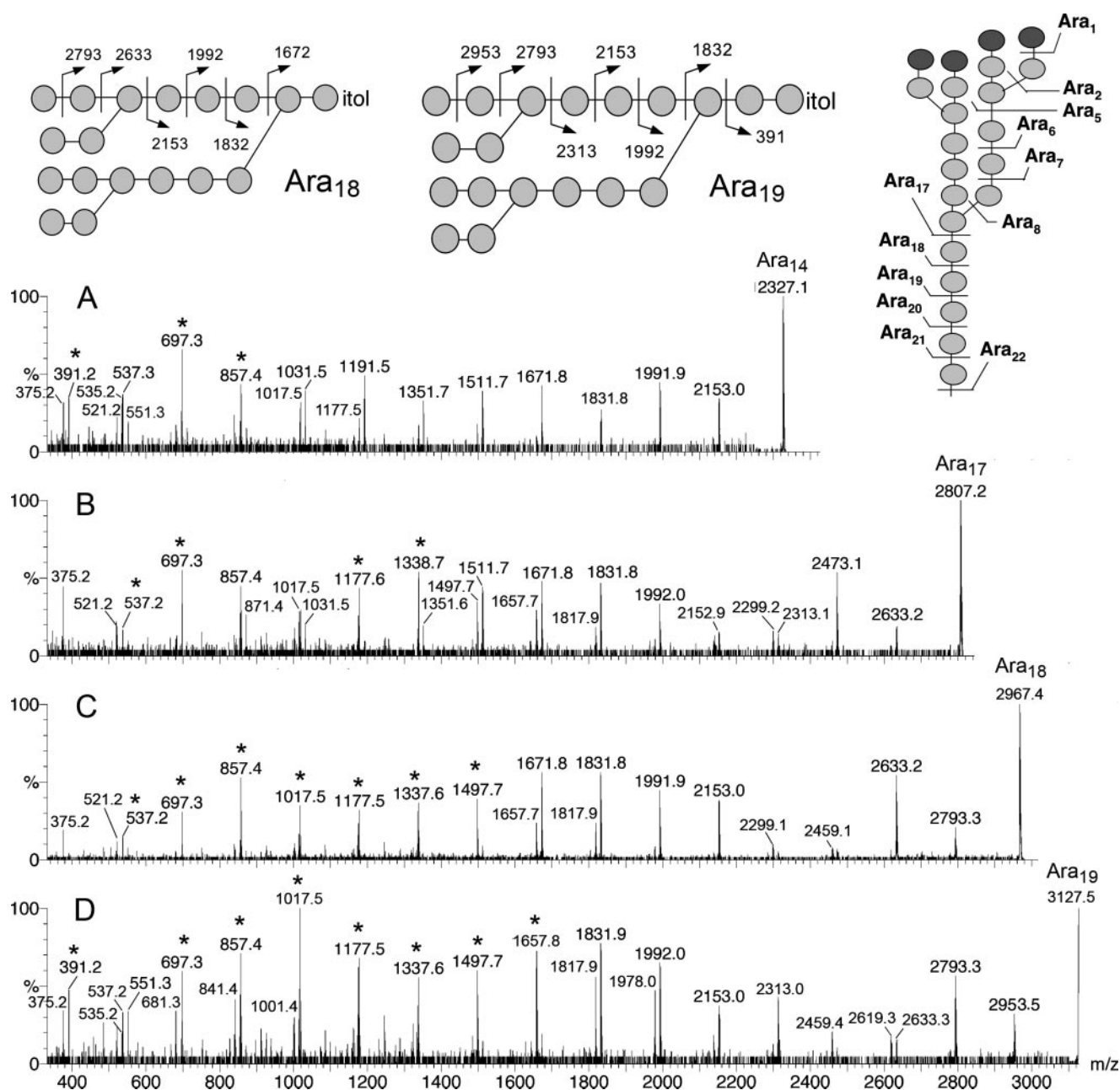


FIGURE 10. MALDI-MS/MS analysis of arabinosyl oligomers derived from *Msm*-arabinanase-digested-truncated LAM of *EmbC*<sub>Δ358c</sub>. Only representative MS/MS spectra on Ara<sub>14</sub>, Ara<sub>17</sub>, Ara<sub>18</sub>, and Ara<sub>19</sub> are shown. Most fragment ions produced are similar to those afforded by the wild-type LAM (Fig. 8). The most significant ions are those produced via single cleavage as indicated on the schematic drawings for Ara<sub>18</sub> and Ara<sub>19</sub>. Peaks marked with an asterisk are those derived from double cleavages for which the corresponding single cleavage ions were not favored and not observed. The sets of fragment ions registered for Ara<sub>18</sub> and Ara<sub>19</sub> are consistent with the Ara<sub>22</sub> oligomer model as shown in the drawing (top right) for which single cleavage nonreducing terminal fragment ions (as indicated on the drawing) can only be derived for a certain arabinosyl composition. MS/MS data for Ara<sub>17</sub> oligomer are consistent with several isomeric structures lacking one of the nonreducing terminal or internal Ara residues but preserving the branched point at the second residue from the reducing end, as in Ara<sub>18</sub>.

by LAM-specific antibody CS-35 were detected. The significant decrease in the abundance of linear Ara<sub>4</sub> in LAM as obtained by the *Cellulomonas* endoarabinanase digestion, however, suggested a dramatic alteration in the terminal end. More importantly, the use of the endogenous *Msm*-arabinanase provided us with an advantage to examine for the first time the arabinan structures beyond just the non-reducing terminal motifs.

Larger oligoarabinosyl fragments could be obtained and readily defined by MALDI-MS and MS/MS analyses, which enabled us to show that the branched terminal Ara<sub>6</sub> motif is

carried on an Ara<sub>18</sub> that descends from the Ara<sub>22</sub>-mer described many years ago in a seminal study on AG (7). For years it was believed that this Ara<sub>18</sub> (Fig. 11) was only present in AG, and three such motifs completed the AG-arabinan, whereas the arabinan of LAM was less structured. On the other hand, the terminal Ara<sub>4</sub> motif arises from linear stretches of arabinan, which is the hallmark of LAM arabinan only. All the structural evidence now points to the arabinan of LAM as a composite of both linear terminal stretches and an AG-like branched Ara<sub>18</sub> core unit. However, how these are distributed

## Arabinan Chain Length Extension in LAM

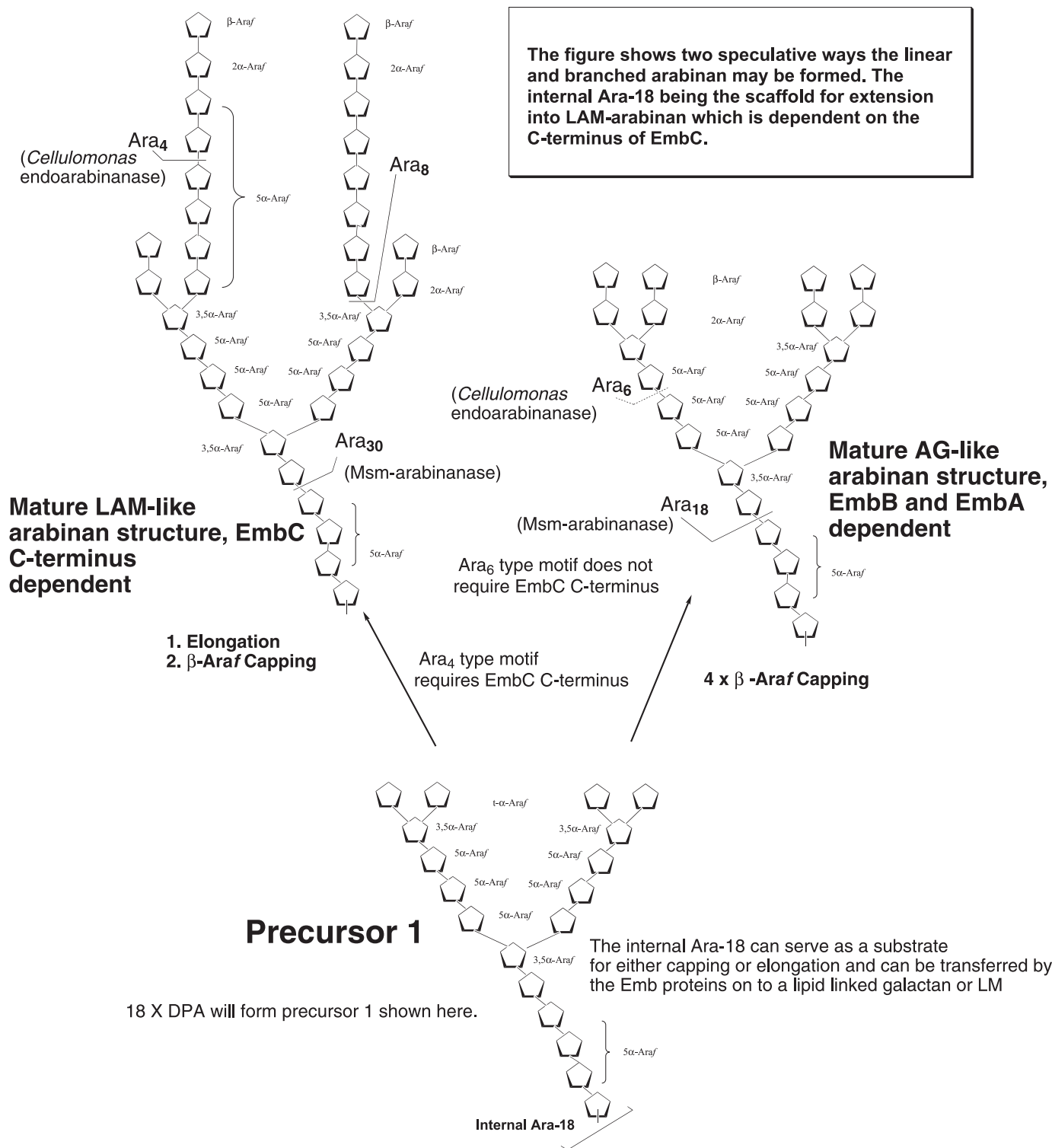


**FIGURE 11. Model for assembly of arabinan of LAM.** The model is based on the information obtained from various structural annotations and functional consequence of genetically manipulated EmbC protein and, therefore, is a "proof of concept" at this stage of our work. Biochemically this has not been established yet. Ara<sub>18</sub> and Ara<sub>30</sub> can be released intact by digestion with Msm-arabinanase. The specificity of this enzyme with respect to possible cleavages at other sites is currently not well established. Ara<sub>4</sub> and Ara<sub>6</sub> can be liberated with the *Cellulomonas* endoarabinanase. There is no structural evidence for Precursor 1, although it is drawn showing 18 Ara<sub>f</sub> residues. This must not be confused with Ara<sub>18</sub> (referred to the structure liberated by Msm-arabinanase). Precursor 1 has no  $\beta$ -Araf capping, a crucial event of chain termination. DPA, decaprenylphosphorylarabinose.

on the mannan backbone is unclear. Our present data establish for the first time that the nonreducing terminal linear extension from any branched point ( $\alpha$ 3,5-Ara<sub>f</sub>) is up to eight or nine Ara<sub>f</sub> residues (as shown in Fig. 11). In wild-type LAM, a vast range of

heterogeneity in size is apparent. The detection of up to Ara<sub>30</sub> among the Msm-arabinanase digest indicates that a portion of the precursor 1 (which is also drawn as 18 Ara<sub>f</sub> residues but could be of a different size) is further extended and would be

consistent with a structural model depicted in Fig. 11. Because various degrees of linear extension coexist with the branched Ara<sub>6</sub> terminal motif carried on the quintessential Ara-18 unit, a full range of digestion products would, thus, be predictably derived as demonstrated in this study. Each Ara<sub>n</sub> detected is furthermore a composite of various isomers and, therefore, could not give a distinctive MS/MS fragmentation pattern.

The noticeable reduction of a significant portion of the linear arabinan stretches could be inferred as the primary lesion leading to truncation in size of LAM made by the recombinant strains containing EmbC derivatives with C-terminal deletions. As a consequence the overt phenotype is manifested as AG-like since the Ara<sub>18</sub> unit became the primary default product in the absence of further extension. It should, however, be noted that unlike the arabinan of AG, a significant portion of the truncated arabinans thus formed was not terminated with  $\beta$ -Araf. Our NMR data clearly showed the appearance of terminal  $\alpha$ -Araf otherwise not found on wild-type LAM or AG. Thus, irrespective of the contribution of *in vivo* arabinanase activity, the wild-type LAM digest product presented is quite clear from Fig. 8 where up to Ara<sub>30</sub> oligomers were obtained. The fact remains that, with EmbC derivatives, we see a distinct profile, which is a positive contribution through biosynthesis, that is impaired when EmbC C terminus is truncated. Remarkably, regardless of the size deletion of the EmbC C terminus, the protein remained functional in effecting the synthesis of the core arabinan in LAM. At present it is not possible to ascertain if the degraded 55-kDa products afforded by EmbC $_{\Delta 200c}$ , EmbC $_{\Delta 300c}$ , EmbC $_{\Delta 368c}$ , and EmbC $_{\Delta 407c}$  were induced during isolation and sample preparation. The respective LAMs made were, however, non-identical. It, thus, indicates that the various mutant constructs did produce functional truncated EmbC proteins *in vivo* that were albeit unstable. More importantly, we have unequivocally shown that the N-terminal region of EmbC alone is sufficient to sustain the capability in making the core arabinan in LAM, perhaps in conjunction with other Emb proteins.

Given the complexity of the structure of the arabinan of LAM and number of arabinosyltransferases required in forming the Ara-(18–22) and its linear extension, the existence of a coordinated multienzyme complex in growing mycobacterial culture seems to be logical. Decaprenylphosphorylarabinose is the only known Araf donor (9, 47) described. If we draw an analogy of the LAM synthesis with LPS synthesis, the Emb proteins could act in arabinan assembly involving a long chain of 5-linked Araf on a C<sub>50</sub>-P-Araf, which has been already translocated across the plasma membrane (48, 49).

In our current working biosynthesis model (Fig. 11), we postulate that an intermediate comprising of  $\alpha$ -linked Araf (Precursor 1 in Fig. 11) units is pre-synthesized from several decaprenylphosphorylarabinose units and ligated to either LM- or lipid-linked galactan. The ligation is dependent on the N-terminal domain of the Emb proteins. AG *versus* LAM biosynthetic pathways may then segregate, as it would require distinct enzymatic attributes to linear extend *versus*  $\beta$  capping of the  $\alpha$ -linked Araf precursor. We have shown that for LAM, this linear extension is dependent on the C-terminal domain of EmbC. In the wild-type strain this would give rise to as large as

an Ara<sub>30</sub> oligomer upon Msm-arabinanase digestion corresponding to the upper end of size distribution of the digestion products detected by MALDI-MS. Other LAM-type arabinan variants may have less extensive linear extension or with none or only one of the possible four termini of Precursor 1 extended.

Based on this working model, we further speculate that the Emb proteins may function as dimers (or higher multimers). The preferred dimers in the wild-type strain are likely to be EmbC/EmbC and EmbA/EmbB for the synthesis of LAM and AG, respectively. For the latter, we have been able to demonstrate that EmbA or EmbB alone are unable to transfer the disaccharide  $\beta$ -D-Araf(1 $\rightarrow$ 2)- $\alpha$ -D-Araf onto a synthetic linear acceptor, but this transferase activity is restored when the enzyme source was combined from *M. smegmatis* $\Delta$ embB and *M. smegmatis* $\Delta$ embA mutants.<sup>6</sup>

However, other dimers may exist under circumstances such as the lack of the ideal partner or changes in the C-terminal domain. Conceptually, then, for the EmbC C-terminal deletion mutants reported herein, the active enzymes could conceivably include the N terminus of EmbC that would ligate the arabinan to LM, but the C terminus of EmbA or EmbB failed to commit the further elongation steps. It is surprising that in *M. smegmatis* $\Delta$ embC, which is unable to synthesize LAM, we have never been able to find any arabinan-containing precursors such as the Precursor 1 in Fig. 11. This can be rationalized as (a) there could be a rapid turnover of these metabolites, (b) degradation of the intermediate arabinan occurs with the endogenous Msm-arabinanase, and most likely, (c) EmbC works in concert with other proteins and utilizes the intermediates. The third possibility is currently being addressed.

All glycosyltransferases with dependence for a polyprenol-linked sugar substitute (proteins of glycosyltransferase superfamily C) have so far been predicted to contain multimembrane-spanning domains. A stage is now set to track down these elusive arabinan intermediates and arabinosyltransferases. We expect most or all of the proteins involved in the arabinan synthesis to be integral membrane proteins with membrane-spanning domains. Acceptors with structures resembling to Precursor 1 are now being chemically synthesized, so that assays can be developed in the future for chain length elongation or capping to substantiate the hypothetical model presented in this work.

*Acknowledgments*—We gratefully acknowledge Dr. Vincent Escuyer for providing the *M. smegmatis* $\Delta$ embC, Dr. Dean Crick for valuable scientific discussions, Dr. Yufang Ma for initial help with genetics, and Christopher Rithner for performing the NMR experiments. Mass spectrometry analyses were performed at the Core Facilities for Proteomics Research located at the Institute of Biological Chemistry, Academia Sinica, supported by a Taiwan National Science Council Grants 93-3112-B-001-010-Y and 94-3112-B-001-009-Y and the Academia Sinica.

## REFERENCES

1. Crick, D. C., Mahapatra, S., and Brennan, P. J. (2001) *Glycobiology* **11**, 107–118
6. S. Khasnobis, J. Zhang, S. Angala, A. Amin, M. McNeil, D. Crick, and D. Chatterjee, unpublished result.

2. Brennan, P. J., and Besra, G. S. (1997) *Biochem. Soc. Trans.* **25**, 188–194
3. Brennan, P. J., and Nikaido, H. (1995) *Annu. Rev. Biochem.* **64**, 29–63
4. Dover, L. G., Cerdeno-Tarraga, A. M., Pallen, M. J., Parkhill, J., and Besra, G. S. (2004) *FEMS Microbiol. Rev.* **28**, 225–250
5. McNeil, M. R., Robuck, K. G., Harter, M., and Brennan, P. J. (1994) *Glycobiology* **4**, 165–173
6. McNeil, M., Daffe, M., and Brennan, P. J. (1991) *J. Biol. Chem.* **266**, 13217–13223
7. Besra, G. S., Khoo, K.-H., McNeil, M. R., Dell, A., Morris, H. R., and Brennan, P. J. (1995) *Biochemistry* **34**, 4257–4266
8. McNeil, M., Daffe, M., and Brennan, P. J. (1990) *J. Biol. Chem.* **265**, 18200–18206
9. Alderwick, L. J., Radmacher, E., Seidel, M., Gande, R., Hitchen, P. G., Dell, A., Sahm, H., Eggeling, L., and Besra, G. S. (2005) *J. Biol. Chem.* **280**, 323362–323370
10. Treumann, A., Xidong, F., McDonnell, L., Derrick, P. J., Ashcroft, A. E., Chatterjee, D., and Homans, S. W. (2002) *J. Mol. Biol.* **316**, 89–100
11. Turnbull, W. B., Shimizu, K. H., Chatterjee, D., Homans, S. W., and Treumann, A. (2004) *Angew. Chem. Int. Ed. Engl.* **43**, 3918–3922
12. Torrelles, J. B., Khoo, K. H., Steling, P. A., Modlin, R. L., Zhang, N., Marques, A. M., Treumann, A., Rithner, C. D., Brennan, P. J., and Chatterjee, D. (2004) *J. Biol. Chem.* **279**, 41227–41239
13. Khoo, K.-H., and Dell, A. (1990) *Glycobiology* **1**, 83–91
14. Nigou, J., Gilleron, M., Cahuzac, B., Bounéry, J. D., Herold, M., Thurnher, M., and Puzo, G. (1997) *J. Biol. Chem.* **272**, 23094–23103
15. Chatterjee, D., Bozic, C. M., McNeil, M., and Brennan, P. J. (1991) *J. Biol. Chem.* **266**, 9652–9660
16. Chatterjee, D., Khoo, K.-H., McNeil, M. R., Dell, A., Morris, H. R., and Brennan, P. J. (1993) *Glycobiology* **3**, 497–506
17. Khoo, K.-H., Dell, A., Morris, H. R., Brennan, P. J., and Chatterjee, D. (1995) *J. Biol. Chem.* **270**, 12380–12389
18. Cole, S. T., Brosch, R., and Parkhill, J. (1998) *Nature* **393**, 537–544
19. Belanger, A. E., Besra, G. S., Ford, M. E., Mikusova, K., Belisle, J. T., Brennan, P. J., and Inamine, J. M. (1996) *Proc. Natl. Acad. Sci. U. S. A.* **93**, 11919–11924
20. Telenti, A., Philipp, W. J., Sreevatsan, S., Bernasconi, C., Stockbauer, K. E., Wieles, B., Musser, J. M., and Jacobs, W. R., Jr. (1997) *Nat. Med.* **3**, 567–570
21. Lety, M. A., Nair, S., Berche, P., and Escuyer, V. (1997) *Antimicrob. Agents Chemother.* **41**, 2629–2633
22. Escuyer, V. E., Lety, M. A., Torrelles, J. B., Khoo, K. H., Tang, J. B., Rithner, C. D., Frehel, C., McNeil, M. R., Brennan, P. J., and Chatterjee, D. (2001) *J. Biol. Chem.* **276**, 48854–48862
23. Zhang, N., Torrelles, J. B., McNeil, M. R., Escuyer, V. E., Khoo, K. H., Brennan, P. J., and Chatterjee, D. (2003) *Mol. Microbiol.* **50**, 69–76
24. Becker, A., and Puhler, A. (1998) *J. Bacteriol.* **180**, 395–399
25. Daniels, C., and Morona, R. (1999) *Mol. Microbiol.* **34**, 181–194
26. Liu, J., and Mushegian, A. (2003) *Protein Sci.* **12**, 1418–1431
27. Berg, S., Starbuck, J., Torrelles, J. B., Vissa, V. D., Crick, D. C., Chatterjee, D., and Brennan, P. J. (2005) *J. Biol. Chem.* **280**, 5651–5663
28. Snapper, S. B., Melton, R. E., Mustafa, S., Kieser, T., and Jacobs, W. R., Jr. (1990) *Mol. Microbiol.* **4**, 1911–1919
29. Spencer, J. S., Kim, H. J., Marques, A. M., Gonzalez-Juarerro, M., Lima, M. C., Vissa, V. D., Truman, R. W., Gennaro, M. L., Cho, S. N., Cole, S. T., and Brennan, P. J. (2004) *Infect. Immun.* **72**, 3161–3170
30. Khoo, K. H., Douglas, E., Azadi, P., Inamine, J. M., Besra, G. S., Mikusová, K., Brennan, P. J., and Chatterjee, D. (1996) *J. Biol. Chem.* **271**, 28682–28690
31. Prinzi, S., Chatterjee, D., and Brennan, P. J. (1993) *J. Gen. Microbiol.* **139**, 2649–2658
32. Chatterjee, D., Lowell, K., Rivoire, B., McNeil, M., and Brennan, P. J. (1992) *J. Biol. Chem.* **267**, 6234–6239
33. McNeil, M., Chatterjee, D., Hunter, S. W., and Brennan, P. J. (1989) *Methods Enzymol.* **179**, 215–242
34. Xin, Y., Huang, Y., and McNeil, M. R. (1999) *Biochim. Biophys. Acta* **1473**, 267–271
35. Dong, X., Bhamidi, S., Scherman, M., Xin, Y., and McNeil, M. R. (2006) *Appl. Environ. Microbiol.* **72**, 2601–2605
36. Dell, A., Reason, A. J., Khoo, K. H., Panico, M., McDowell, R. A., and Morris, H. R. (1994) *Methods Enzymol.* **230**, 108–132
37. Kaur, D., Lowary, T. L., Vissa, V. D., Crick, D. C., and Brennan, P. J. (2002) *Microbiology* **148**, 3049–3057
38. Gilleron, M., Himoudi, Adam, O., Constant, O., Constant, P., Vercellone, A., Riviere, M., and Puzo, G. (1997) *J. Biol. Chem.* **272**, 117–124
39. Lee, R. E., Li, W., and Chatterjee, D. (2005) *Glycobiology* **15**, 139–151
40. Nigou, J., Vercellone, A., and Puzo, G. (2000) *J. Mol. Biol.* **299**, 1373–1382
41. Delmas, C., Gilleron, M., Brando, T., Vercellone, A., Gheorghiu, M., Riviere, M., and Puzo, G. (1997) *Glycobiology* **7**, 811–817
42. Gibson, K. J., Gilleron, M., Constant, P., Puzo, G., Nigou, J., and Besra, G. S. (2003) *Microbiology* **149**, 1437–1445
43. Besra, G. S., Khoo, K.-H., Belisle, J. T., McNeil, M. R., Morris, H. R., Dell, A., and Brennan, P. J. (1994) *Carbohydr. Res.* **251**, 99–114
44. Chatterjee, D., and Khoo, K. H. (1998) *Glycobiology* **8**, 113–120
45. Strohmeier, G. R., and Fenton, M. J. (1999) *Microbes Infect.* **1**, 709–717
46. Briken, V., Porcelli, S. A., Besra, G. S., and Kremer, L. (2004) *Mol. Microbiol.* **53**, 391–403
47. Wolucka, B. A., McNeil, M. R., de Hoffmann, E., Chojnacki, T., and Brennan, P. J. (1994) *J. Biol. Chem.* **269**, 23328–23335
48. Raetz, C. R. H., and Whitfield, C. (2002) *Annu. Rev. Biochem.* **71**, 635–700
49. Clarke, B. R., Cuthbertson, L., and Whitfield, C. (2004) *J. Biol. Chem.* **279**, 35709–35718
50. Kall, L., Krogh, A., and Sonnhammer, E. L. (2004) *J. Mol. Biol.* **338**, 1027–1036
51. von Heijne, G. (1992) *J. Mol. Biol.* **225**, 487–494